Automatic tuning of grid forming controls considering passivity and dynamic performance

Eros Avdiaj
Department of Electrical Engineering
KU Leuven, Etch
Leuven, Genk, Belgium
ORCID: 0000-0003-1802-3342

Matteo Rossini
Department of Electrical Engineering
KU Leuven, Etch
Leuven, Genk, Belgium
ORCID: 0000-0002-3202-9903

Jef Beerten
Department of Electrical Engineering
KU Leuven, Etch
Leuven, Genk, Belgium
ORCID: 0000-0002-8756-2983

***Abstract*—The increasing deployment of grid-forming converters (GFMs) in modern power systems requires control designs that ensure system support and robust stability under changing grid conditions. Achieving this for each new connection, however, is a time-intensive process. This paper proposes an automated tuning method that streamlines the control design of GFMs by embedding both essential voltage source (EVS) characteristics and passivity constraints into an optimization framework. The method determines the control parameters that achieve a desired effective impedance and ensure converter passivity up to a specified frequency range. Analytical and electromagnetic transient (EMT) simulation results demonstrate that the proposed approach consistently attains the target EVS behavior while preserving stability robustness, offering a systematic tool for the practical deployment of grid-forming converters.**

***Index Terms*—Grid forming, Optimization**

I. Introduction

The increasing integration of grid-forming (GFM) converters in modern power systems requires control designs that simultaneously provide dynamic system support and maintain robust stability under varying grid conditions. Converter specifications are typically defined by transmission system operators (TSOs), which vary by connection point, necessitating frequent retuning as the number of GFM projects grows.

The behavior of grid-forming (GFM) converters is determined by their self-synchronization mechanisms, implemented in the outer synchronization loops, and by their instantaneous active and reactive current responses to voltage magnitude and phase perturbations, governed by the inner control loops. These instantaneous responses are typically represented using the voltage-source-behind-impedance (VSBI) model. Recent GFM requirements [1] define effective impedance ranges that capture both the converter's physical impedance and the dynamic impedance introduced by its control actions under grid variations.

In addition to VSBI behavior, the converters are expected to have a positive passivity index at frequencies other than the fundamental [2]. The passivity index enables an independent frequency-wise assessment of converter stability and robustness without requiring prior knowledge of the external grid. The inner control loops of GFM converters shape both the essential voltage source (EVS) characteristics and the system's passivity. Tuning of these parameters is challenging, particularly when maintaining the desired effective impedance and a positive passivity index across a wide frequency range. Currently, there are no explicit guidelines for tuning converter control parameters.

Previous work by the authors [3] introduced a passivity-based design of the Current-Controlled Virtual Synchronous Machine (CC-VSM). However, selecting suitable control parameters remains complex and time-consuming, limiting scalability across multiple converters and grid conditions. An automated tuning approach could overcome this challenge; yet, to the best of the authors' knowledge, no existing methods simultaneously address VSBI and passivity constraints.

To overcome this limitation, this paper proposes an automated tuning method that optimizes converter control parameters to achieve a predefined effective impedance while preserving desired EVS characteristics and passivity. The proposed framework offers a systematic, scalable solution for GFM control design, explicitly supporting system requirements at the point of connection.

The paper is organized as follows: Section II outlines the methodology based on passivity, EVS characterization, and optimization; Section III details the passive control design of the MMC-based GFM converter; Section IV describes the optimization process and constraints; Section V presents the results; and Section VI concludes the paper.

II. Methodology

A. Passivity

Passivity is a property of systems that do not generate energy, ensuring inherent stability and robustness. Passivity-based control exploits this feature, enabling GFM converters to act as passive elements, promoting stable grid interactions. If all components in an interconnected system are passive, the overall system is stable. Although conservative, passivity-oriented design provides a sufficient, grid-independent stability condition, assuming the external network is also passive.

This work was supported by the Research Foundation – Flanders (FWO) [grant number 12AGN26N] and by the project *Innovative solutions for underground high-voltage lines and grids*, funded by the Flemish Government.

979-8-3315-8138-1

The passivity of power electronic converters is commonly assessed through their multi-input-multi-output (MIMO) small-signal admittance matrix, $\mathbf{Y}$, defined as

$$\Delta\mathbf{i} = \mathbf{Y}(s)\,\Delta\mathbf{v} \tag{1}$$

where $\Delta\mathbf{i}$ is the small-signal current entering the converter and $\Delta\mathbf{v}$ is the small-signal voltage perturbation at the point of common coupling (PCC). A converter is passive if the passivity index is positive,

$$\lambda_{min}(\mathbf{Y}(j\omega) + \mathbf{Y}^H(j\omega)) > 0, \quad \forall\omega \tag{2}$$

where H denotes the Hermitian (complex conjugate transpose) operator and λ_{min} represents the minimum eigenvalue.

In practice, full passivity across all frequencies is rarely achievable, as converters must supply power and act as sources at low frequencies. Hence, the converter is designed to remain dissipative and maintain a positive passivity index outside the bandwidth of the outer control loops, ensuring stable dynamic interactions with the grid.

B. Essential voltage source characteristics

Collaborative efforts between academia and industry [1] have defined the VSBI behavior as a fundamental requirement for GFM converters. This behavior specifies the instantaneous active and reactive current responses to perturbations in the PCC's voltage angle θ and magnitude v. According to [1], the converter's dynamic response is characterized by an effective impedance x_{eff}, which determines the response between voltage perturbations and current changes (e.g., $\Delta i_q \approx 1/x_{\text{eff}} \cdot \Delta v$). Typical x_{eff} ranges are 0.25–0.35 pu for medium-voltage and 0.4–0.5 pu for high-voltage systems, with a minimum rise time of $t_r = 10$ ms. This effective impedance must be ensured up to the bandwidth of the outer GFM loops, ω_{GFM}.

The frequency-domain power flow Jacobian [4] relates small-signal power variations to voltage perturbations through the converter's dq-admittance matrix as

$$\mathbf{J}(s) = \begin{bmatrix} \frac{p(s)}{v(s)/v_0} & \frac{p(s)}{\theta(s)} \\ \frac{q(s)}{v(s)/v_0} & \frac{q(s)}{\theta(s)} \end{bmatrix} = \frac{3}{2}v_0^2 \begin{bmatrix} Y_{dd}(s) & Y_{dq}(s) \\ -Y_{qd}(s) & -Y_{qq}(s) \end{bmatrix} + \begin{bmatrix} p_0 & -q_0 \\ q_0 & p_0 \end{bmatrix}. \tag{3}$$

This holds for the amplitude-invariant Park transform, with the d-axis alignment and the q-axis leading by 90°. For the derivation of (3), the readers are referred to the appendix in [4]. The off-diagonal terms Y_{dq} and Y_{qd} capture specifically the active power sensitivity to voltage angle and the reactive power sensitivity to voltage magnitude. Based on (3) and following the GFM requirements from [1], [2], three essential voltage source characteristics are identified in [4] and recalled as:

1) R1: The magnitudes of Y_{dq} and Y_{qd} should lie between $6-12$ dB, corresponding to $1/x_{\text{eff}}$ for the recommended impedance.
2) R2: The phases of $p(s)/\theta(s)$ and $q(s)/v(s)$ must ensure positive system support, thus they should be within $\pm 90°$.
3) R3: The dq-frame admittance matrix has a positive passivity index beyond the outer loop bandwidth (i.e., $\omega > \omega_{\text{GFM}}$).

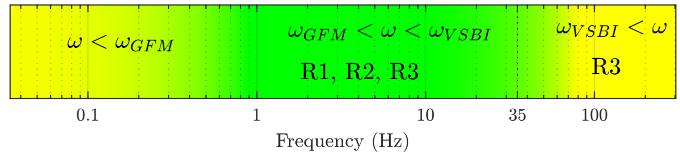

Fig. 1. Bounds of the essential voltage source characteristics.

These characteristics define the desired frequency domain characteristics of any GFM control strategy that delivers instantaneous VSBI behavior. Since this instantaneous response depends primarily on the inner GFM loops, characteristics R1–R3 apply only within the frequency range $\omega_{\text{GFM}} < \omega < \omega_{\text{VSBI}}$. For $\omega > \omega_{\text{VSBI}}$, only passivity is required up to the maximum frequency of interest $\omega_{\max}$. These frequency-domain regions are illustrated in Fig. 1.

The inner GFM loops responsible for instantaneous behavior have the Y_{dq} and Y_{qd} inversely related to the effective impedance x_{eff}, extending up to the bandwidth ω_{VSBI}. For bandwidth illustration, considering a typical second-order response with damping $\zeta = 0.707$ and rise time $t_r = 10$ ms [1], the natural frequency $\omega_n = \pi/(2t_r\sqrt{1-\zeta^2})$ corresponds to a bandwidth of approximately $\omega_{\text{VSBI}} = 2\pi \times 35$ rad/s.

C. Optimization

The automatic tuning aims to find the best converter control parameters to achieve the desired EVS characteristics without explicitly evaluating every possible parameter combination.

The EVS characteristics cannot be expressed in closed form as a function of the converter control parameters. However, they can be computed numerically for any input as the converter's inner loop control parameters determine its frequency-domain behavior, from which the admittance matrix can be derived. The resulting EVS characteristics can then be quantified by evaluating this admittance.

Hence, a "simulation optimization" approach [5] is required. An optimization problem is defined with the converter control parameters as input variables. Its objective is to minimize the deviation from a target effective impedance x_{eff}, subject to constraints that ensure the EVS characteristics are satisfied.

III. Electrical model and control

The system configuration presented in Fig. 2 is utilized to show the effectiveness of the optimization. In this structure, an MMC operated as a current-controlled virtual synchronous machine (CC-VSM) is connected to a local power system, which is represented as a Thevenin equivalent. In this figure, uppercase symbols indicate physical variables or parameters, while lowercase symbols indicate per-unit quantities or parameters utilized by the VSM-based control. The converter model and control are based on [3], where the paper discusses a passivity method and presents the design for passive inner GFM loops. The main elements important for this paper are presented below. For more information regarding the parameters and modeling, the reader is referred to [3].

The converter's AC-side response is highly impacted by the inner loops, namely, the virtual impedance and current

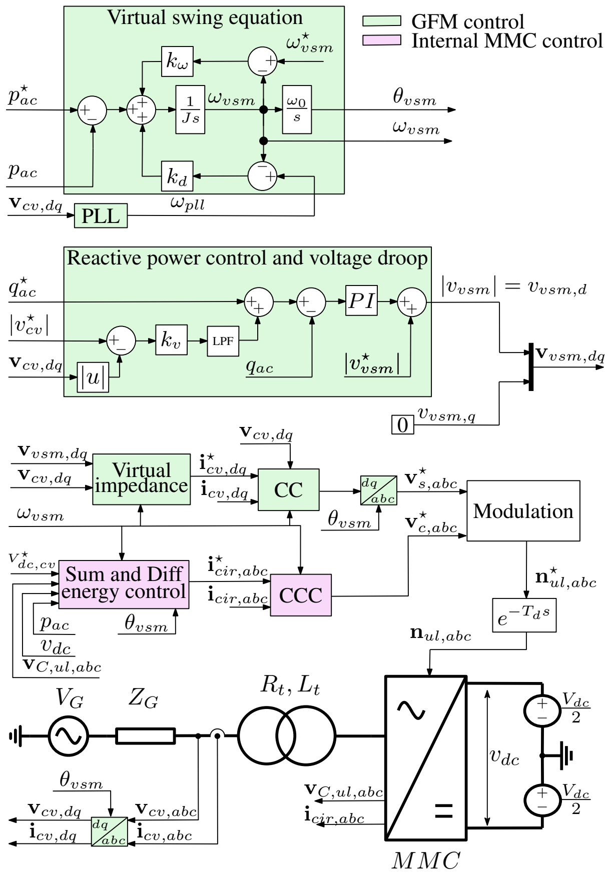

Fig. 2. Control of the MMC-based GFM converter.

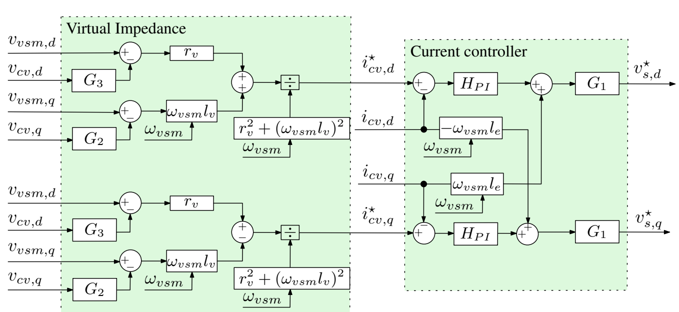

Fig. 3. Block diagram of the inner CC-VSM's loops.

controller. A detailed representation of these structures is presented in Fig. 3. Here, l_v and r_v are the virtual inductance and resistance, respectively, ω_{vsm} is the angular rotating frequency of the VSM, l_e is the equivalent arm impedance, including half the arm impedance and transformer impedance, H_{PI} is the current controller transfer function as $(k_i + k_p s)/s$. In addition to these standard elements, there are also G_1, G_2, and G_3. The compensator G_1 is a lead-lag filter utilized to compensate for the time delays in the higher frequency range by introducing a phase shift α_1 at frequency $f_1 = 2\pi\omega_1$. The

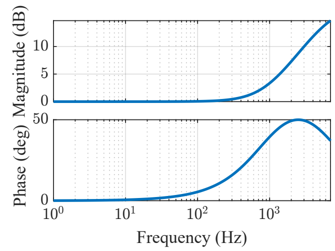

Fig. 4. Bode plot of G_1.

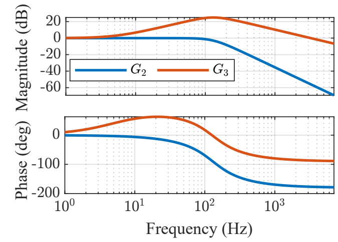

Fig. 5. Bode plot of G_2 and G_3.

transfer function of this compensator is

$$\alpha_{\text{lead}} = \frac{1+\sin(\alpha_1)}{1-\sin(\alpha_1)}, \qquad P_1 = \omega_1\sqrt{\alpha_{\text{lead}}}, \tag{4}$$

$$G_1(s) = \alpha_{\text{lead}}\frac{s + P_1/\alpha_{\text{lead}}}{s + P_1}, \tag{5}$$

while the Bode plot of this transfer function is given in Fig. 4.

The compensators G_2 and G_3 are given as

$$G_2 = \frac{\omega_{lpf,2}^2}{s^2 + 2\xi_{lpf,2}\omega_{lpf,2}s + \omega_{lpf,2}^2}, \tag{6}$$

$$G_3 = \frac{\frac{\omega_{lpf,3}^2}{\omega_{hpf,3}}s + \omega_{lpf,3}^2}{s^2 + 2\xi_{lpf,3}\omega_{lpf,3}s + \omega_{lpf,3}^2}. \tag{7}$$

The compensator G_2 is a second-order low-pass filter which serves to reduce the impact of the virtual inductance at higher frequencies. It was demonstrated in [3] that G_2 limits the Y_{dq} and Y_{qd} at higher frequencies, thus directly impacting the "instantaneous" response of the VSBI behavior. Simultaneously, it affects the passivity index of the admittance matrix. Meanwhile, G_3 is a second-order low-pass filter and a high-pass filter which serves to limit the impact of the virtual resistance at higher frequencies while increasing dissipation and maintaining a positive passivity index. The Bode plots of G_2 and G_3 are presented in Fig. 5.

The tuning of virtual impedance l_V, r_v, and compensators G_1, G_2, and G_3, directly impacts the EVS characteristics and the passivity of the system. The exact parameter selection process is laborious, as explained in [3], and it cannot easily scale if several converters have to be quickly designed for different grid responses. Moreover in [3], to reduce the complexity the following constrains were added, $\omega_{lpf,3} = \omega_{lpf,2}$ and $\xi_{lpf,3} = \xi_{lpf,2}$; however, lifting these constraints allows for higher degrees of freedom, which can result in better tuning parameters. Therefore, for these reasons, an automated tuning method is proposed in the next section.

IV. Automated Tuning

Multiple control parameters simultaneously affect the converter's passivity and VSBI behavior. The design objective is to realize a desired "instantaneous" response, defined by the target effective impedance x_{eff} and the bandwidth ω_{VSBI}. This response should be ensured while maintaining the passivity of the inner loops up to a predefined frequency $\omega_{\max}$. To evaluate

979-8-3315-8138-1

the EVS characteristics and the passivity, we utilize the analytical model presented in [3]. Numerical evaluations use log-spaced discrete frequencies $\{\omega_i\}_i \subset [0, \omega_{\max}]$; nevertheless, we treat frequency as continuous for notational clarity. Given that inner GFM loops are designed to be symmetrical (i.e., $Y_{dd}(s) = Y_{qq}(s)$ and $Y_{dq}(s) = -Y_{qd}(s)$), we consider only $Y_{dd}(s)$ and $Y_{dq}(s)$ in the following.

A. Identification of the tuning parameters

Different GFM structures feature distinct tunable parameters. In the proposed design, the inner loop depends on the PI current controller, virtual impedance, and filter or compensator parameters (G1, G2, G3). The PI controller is preset to ensure the desired current performance and reference tracking under saturation. Hence, only the remaining elements are tuned to achieve the desired EVS characteristics while maintaining passivity. Therefore, the set of design parameters is $\mathbf{k} = \{l_v, r_v, \omega_1, \alpha_1, \omega_{lpf,2}, \xi_{lpf,2}, \omega_{hpf,3}, \omega_{lpf,3}, \xi_{lpf,3}\}$.

B. Objective function

The objective of the optimization problem is to minimize the error between the minimum $|Y_{dq}|$ up to the bandwidth ω_{VSBI} and the expected response of the effective impedance,

$$\text{minimize} \quad f(\mathbf{k}) = \left| \left(\min_{\omega \in [0, \omega_{\mathrm{VSBI}}]} |Y_{dq}(j\omega)| \right) - 1/x_{\mathrm{eff}} \right|. \quad (8)$$

The design parameters $\mathbf{k}$, although not represented explicitly in the expression above, determine the value of $Y_{dq}(j\omega)$.

C. Constraints

1) Passivity constraint: Nonnegativity of passivity index up to $\omega_{\max}$ is enforced by

$$\lambda_{\min}\big(Y(j\omega) + Y^H(j\omega)\big) \geq 0 \quad \forall\, \omega \in [0, \omega_{\max}]. \quad (9)$$

2) Converter support constraints: The EVS characteristic is defined by the magnitude and phase of Y_{dq}. Specifically, $\angle Y_{dq}$ should be within $\pm 90^\circ$ up to ω_{VSBI},

$$-90^\circ \leq \angle Y_{dq}(j\omega) \leq 90^\circ \quad \forall\, \omega \in [0, \omega_{\mathrm{VSBI}}]. \quad (10)$$

3) Admittance attenuation constraints: To ensure practical implementability, the converter admittance is constrained to attenuate at higher frequencies. This prevents amplification of noise, switching ripple, and unmodeled dynamics. The constraint is practically achieved as

$$|Y_{dd}(j\omega_{\max})|_{\mathrm{dB}} \leq -10 \text{ dB}, \quad (11)$$

$$|Y_{dq}(j\omega_{\max})|_{\mathrm{dB}} \leq -10 \text{ dB}, \quad (12)$$

$$|Y_{dd}(j\omega_{\max})| \leq |Y_{dd}(j(\omega_{\max} - 10))|, \quad (13)$$

$$|Y_{dq}(j\omega_{\max})| \leq |Y_{dq}(j(\omega_{\max} - 10))|. \quad (14)$$

D. Optimization algorithm

The optimization problem is nonconvex, with a nonlinear objective and nonlinear constraints, and the gradients of both are unavailable. Thus, a derivative-free optimization algorithm is required.

We employ a direct search augmented Lagrangian algorithm based on [6]. Our experiments indicate that the objective landscape is rugged. High-quality solutions can be obtained by constraining the search region with bounds on all optimization variables – guided by engineering judgment – and by adopting a randomized multistart strategy.

V. Results

The effective impedance x_{eff} is considered the primary input defining the desired EVS characteristic. To evaluate the performance of the proposed automated tuning method, three converter designs are compared. Case 1 (base case) follows the design in [3], targeting an effective impedance of $x_{\mathrm{eff}} = l_v \omega_{vsm} = 0.375$ pu. For Case 2, the virtual impedance is reduced to achieve a more pronounced VSBI behavior with $l_v \omega_{vsm} = x_{\mathrm{eff}} = 0.25$ pu, while maintaining the same tuning for the other parameters as in Case 1. Lastly, in Case 3, the converter parameters are obtained using the automated tuning method proposed in Section IV, with input of $x_{\mathrm{eff}} = 0.25$ pu, $\omega_{\mathrm{VSBI}} = 2\pi \times 50$ rad/s, and $\omega_{\max} = 2.5$ kHz. The optimization yields $r_v = 0.0083$ pu, $l_v = 0.255$ pu, $\omega_1 = 5.1 \times 10^4$ rad/s, $\alpha_1 = 53^\circ$, $\omega_{lpf,2} = 2\pi \times 80.7$ rad/s, $\xi_{lpf,2} = 0.605$, $\omega_{lpf,3} = 2\pi \times 61$ rad/s, $\omega_{hpf,3} = 0.04\omega_{lpf,3}$, and $\xi_{lpf,3} = 0.566$. The performance of the three designs is first analyzed using the analytical small-signal model, which captures only the inner current control loops of the CC-VSM as in [3]. The same cases are then evaluated using a full MMC-based grid-forming converter model implemented in electromagnetic transient (EMT) simulations. The converter's frequency-domain admittance is obtained via the Z-Tool by the frequency-scanning technique [7].

Fig. 6 shows results for the analytical frequency-domain admittance matrix $\mathbf{Y}_{dq}$ of the inner GFM loops for the three cases. The terms Y_{dq} and Y_{qd} exhibit higher magnitudes at frequencies below 100 Hz, which are related to the EVS characteristics. The corresponding passivity index, shown in Fig. 7, indicates that Case 1 and Case 3 remain passive across all frequencies, whereas Case 2 becomes nonpassive in certain regions. This demonstrates that modifying the virtual impedance without retuning other control parameters can compromise passivity and reduce robustness to system uncertainties. In contrast, the automated tuning optimizes the control parameters to preserve passivity while maintaining the desired EVS characteristics.

The time-domain validation is presented in Fig. 8, showing the -5% voltage step response derived from the analytical admittances Y_{dd} and Y_{dq}. All designs achieve rise times faster than 10 ms, in agreement with [1]. The steady-state current responses are consistent with the expected effective impedance, e.g., for Case 2 and Case 3, $i_q \approx 0.05/0.25 = 0.2$ pu. As expected, a smaller x_{eff} yields a larger (current) support to the system and higher $|Y_{dq}|$ and $|Y_{qd}|$, whose magnitude in decibels is approximately follow $20\log_{10}(1/x_{\mathrm{eff}})$ up to ω_{VSBI}.

To further validate these findings, the analysis is repeated for the complete control structure shown in Fig. 2. The

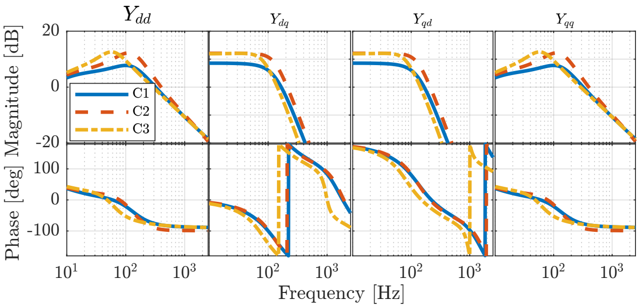

Fig. 6. $\mathbf{Y}_{dq}$ of inner CC-VSM's loop for tuning with Case 1, Case 2, and Case 3.

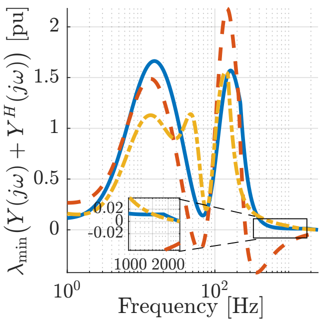

Fig. 7. Passivity index for systems of Fig. 6.

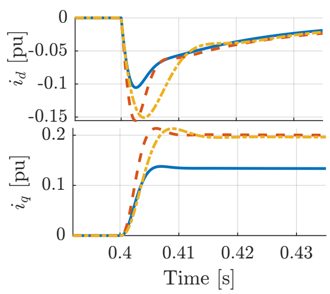

Fig. 8. VSBI response to -5% step in v_d for the systems in Fig. 6.

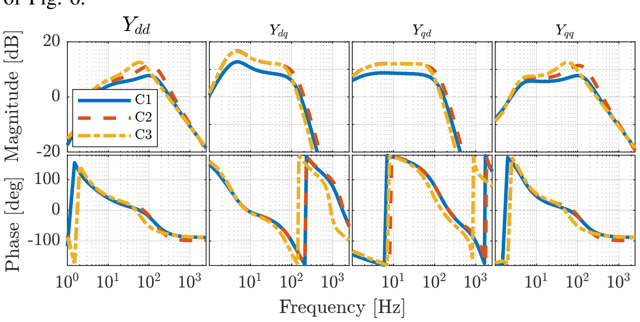

Fig. 9. $\mathbf{Y}_{dq}$ of full GFM-MMC for tuning with Case 1, Case 2, and Case 3.

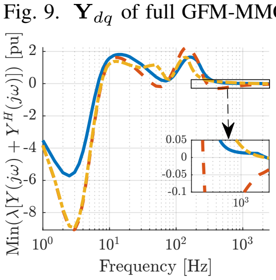

Fig. 10. Passivity index for systems of Fig. 9.

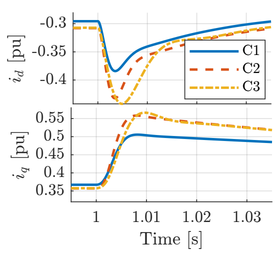

Fig. 11. Time domain response to -5% step in voltage magnitude.

corresponding results, $\mathbf{Y}_{dq}$, the passivity index, and the time-domain responses, are presented in Fig. 9, Fig. 10, and Fig. 11, respectively. The overall trends are consistent with the analytical study. However, by comparing Fig. 7 and Fig. 10, it can be observed that the full control exhibits slight nonpassive behavior at low frequencies, attributed to the influence of the outer GFM control loops.

The proposed automated tuning method achieves the desired EVS characteristics while maintaining converter passivity up to the specified frequency range. This systematic approach aligns with recent grid-forming specifications [1], [2], ensuring tunable dynamic support and robust stability.

VI. Conclusions

This paper presents an automated tuning framework for the control design of grid-forming converters, ensuring both passivity and compliance with essential voltage source characteristics. The method utilizes the desired voltage source behind impedance behavior, characterized by effective impedance and bandwidth specifications, as inputs and automatically determines the control parameters to satisfy the EVS and passivity requirements across the relevant frequency range.

The results demonstrated that only adjusting the virtual impedance can compromise passivity, whereas the proposed optimization consistently achieves the target impedance behavior while maintaining robustness. Analytical and EMT-based validations confirmed that the tuned inner converter loops preserve passivity and provide the expected "instantaneous" response to grid voltage perturbations. The proposed approach offers a systematic and scalable method for GFM control design, aligning with recent grid-forming specifications to ensure dynamic support and robust stability.

Future work may extend the analysis to additional grid codes and standards, such as IEEE 2800, to further generalize and validate the applicability of the proposed approach.

References

[1] ENTSO-E, "Grid forming capability of power park modules: First interim report on technical requirements," European Network of Transmission System Operators for Electricity (ENTSO-E), Tech. Rep., May 2024.

[2] 50Hertz, Amprion, Tennet, TransnetBW, "4-TSO paper on requirements for grid-forming converters," Germany, Tech. Rep., 2024.

[3] E. Avdiaj, D. Lee, O. C. Sakinci, and J. Beerten, "Passivity-based design methodology for current-controlled grid-forming MMCs," *IEEE JESTIE*, vol. 6, no. 4, pp. 1366–1377, 2025. DOI: 10.1109/JESTIE.2025.3585455

[4] E. Avdiaj, "Control design of grid-forming converters: Dynamic and harmonic analysis of grid-forming MMC-based STATCOMs," Ph.D. dissertation, KU Leuven, 2025.

[5] Y. Carson and A. Maria, "Simulation optimization: Methods and applications," in *Proceedings of the 29th Conference on Winter Simulation*, IEEE Computer Society, 1997, pp. 118–126. DOI: 10.1145/268437.268460

[6] T. G. Kolda, R. M. Lewis, and V. J. Torczon, "A generating set direct search augmented lagrangian algorithm for optimization with a combination of general and linear constraints," Sandia National Laboratories, Tech. Rep., Aug. 2006. DOI: 10.2172/893121

[7] F. J. Cifuentes Garcia et al., "Automated frequency-domain small-signal stability analysis of electrical energy hubs," in *2024 IEEE PES ISGT EUROPE*, 2024, pp. 1–6.